

Chaos and Ergodicity in Extended Quantum Systems with Noisy Driving

Pavel Kos,¹ Bruno Bertini,^{1,2} and Tomaž Prosen¹

¹*Department of Physics, Faculty of Mathematics and Physics,
University of Ljubljana, Jadranska 19, SI-1000 Ljubljana, Slovenia*
²*Rudolf Peierls Centre for Theoretical Physics, Clarendon Laboratory,
Oxford University, Parks Road, Oxford OX1 3PU, United Kingdom*
(Dated: October 26, 2020)

We study the time evolution operator in a family of local quantum circuits with random longitudinal fields. We argue that the presence of quantum chaos implies that at large times the time evolution operator becomes effectively a *random matrix* in the many-body Hilbert space. To quantify this phenomenon we compute analytically the squared magnitude of the trace of the evolution operator — the generalised spectral form factor — and compare it with the prediction of Random Matrix Theory (RMT). We show that for the systems under consideration the generalised spectral form factor can be expressed in terms of dynamical correlation functions of local observables in the infinite temperature state, linking chaotic and ergodic properties of the systems. This also provides a connection between the many-body Thouless time τ_{th} — the time at which the generalised spectral form factor starts following the random matrix theory prediction — and the conservation laws of the system. Moreover, we explain different scalings of τ_{th} with the system size, observed for systems with and without the conservation laws.

The concept of *chaos* is very natural in classical systems. Its naive formulation in terms of strong sensitivity of the trajectory to the initial conditions, the “butterfly effect”, is so simple and powerful that has long become an element of the popular culture. During the second half of the twentieth century this concept has been refined, from both the physical and mathematical points of view, leading to a complete theory of chaos in classical dynamical systems [1–4] that can be regarded as one of the greatest achievements of mathematical physics.

In the quantum realm the situation is much less intuitive due to the absence of well defined trajectories and the linear structure of the unitary evolution. In this context, a key role is played by the spectral correlations of the time-evolution operator. Indeed, as established in a series of seminal works [5–7], systems with a well defined chaotic classical limit have a spectrum with correlations that coincide with those of an ensemble of random matrices with the same symmetries. The latter property remains well defined also away from the classical limit and has then been taken as a definition of quantum chaos. However, the problem of connecting the spectral statistics with more intuitive dynamical properties of the system remained open.

Over the last decade the problem of characterising chaos in quantum systems received a renewed interest due to seminal results coming for the study of black holes [8, 9] and connecting quantum many-body chaos with the *scrambling* of quantum information. In turn, this renaissance also led to new discoveries concerning chaos in extended quantum many-body systems on the lattice [10–26] and led to the introduction of useful minimal models like local random unitary circuits [11, 27] and dual-unitary circuits [28]. For some of these systems it has been possible to compute measures of the spectral statistics [10, 12–14, 18], proving that they indeed follow the predictions of Random Matrix Theory. Importantly,

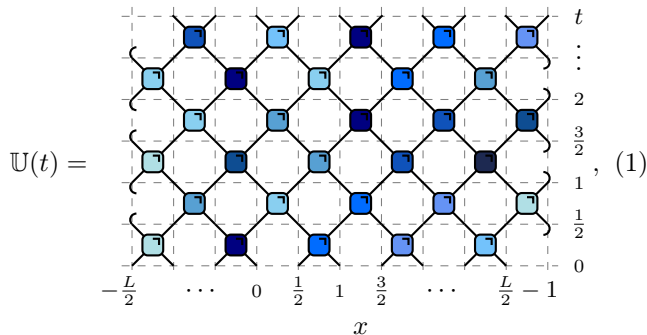
however, it has been realised that in generic extended systems with local interactions this happens only for energy levels smaller than a certain scale E_{th} — known as Thouless Energy — which bares information on the spatial structure. This energy scale (or the associated Thouless time $\tau_{\text{th}} = \hbar/E_{\text{th}}$) is believed to display different scalings with the system size depending on the conservation laws of the system.

In the recent comeback of quantum chaos an important role has been played by driven systems, as they furnish a simpler modelisation of many interesting dynamical phenomena [23–27]. For these systems, in the generic instance of aperiodic driving, the spectral statistics is not well defined (their time-evolution operator is time-dependent) and the chaotic regime has been identified by looking at some features of the quantum many-body dynamics — seeking a quantum many-body analogue of the butterfly effect. Some of the most studied features have been the spreading of support of local operators (measured, e.g., by out-of-time-ordered correlators [29–31]), the growth of complexity in the classical simulations of the dynamics [32], and the scrambling of quantum information [33]. However, even though all these features are connected to an idea of ‘dynamical complexity’, they provide different information. It is unclear what is the minimal set of these features that a system has to display to be considered chaotic.

In this Letter we follow a different route and regard as “chaotic” those driven systems where the time-evolution operator acquires random matrix spectral correlations after a certain initial transient [34, 35]. This is a direct generalisation of the traditional definition of quantum chaos and the transient is naturally interpreted as the Thouless time [35]. We present a family of local quantum circuits with random longitudinal fields for which the time-dependent spectral correlations can be characterised exactly. In particular, we compute the squared

magnitude of the trace of the evolution operator — which we dub Generalised Spectral Form Factor (GSFF) — and show that at the leading order in time it is fully specified by the two-point dynamical correlation functions of local operators in the infinite temperature state. We use this to show that the regime of quantum chaos coincides with the ergodic and mixing one (where all dynamical correlations decay in time). The aforementioned connection also provides a direct link between conservation laws and scaling of the Thouless time with the system size.

More specifically, we consider a chain of length L with $2L$ qubits placed at integer and half-integer indexed sites. Thus, the Hilbert space of the system is $\mathcal{H} = (\mathbb{C}^2)^{\otimes 2L}$. The time evolution is governed by a brickwork local quantum circuit, consisting of unitary matrices (gates) acting on two neighbouring spins (with periodic boundary conditions). We consider the case where the gates are different at each space-time point and represent the time evolution as



$$U(t) = \text{Diagram of brickwork local quantum circuit}, \quad (1)$$

where we depicted two-site gates as

$$U_{x,\tau} = \text{Diagram of two-site gate}, \quad x \in \frac{1}{2}\mathbb{Z}_{2L}, \quad \tau \in \frac{1}{2}\mathbb{Z}_{2t}, \quad x + t \in \mathbb{Z}, \quad (2)$$

and different colours denote different matrices. Note that we adopt the convention of time running upwards.

The main quantity of interest for this paper is the GSFF defined as

$$K_g(t) \equiv \langle |\text{tr}_{\text{sector}} \mathbb{U}(t)|^2 \rangle, \quad t > 0. \quad (3)$$

where the trace is reduced to a common eigenspace of \mathbb{U} and all its commuting symmetries, and $\langle \cdot \rangle$ denotes an average of some sort (either a moving time-average or an average over an ensemble of similar systems). Such an average is necessary because the distribution of $|\text{tr} \mathbb{U}(t)|^2$ in an ensemble of systems does *not* generically become infinitely peaked even in the limit of infinitely many degrees of freedom, but maintains non-trivial tails (for example, this is the case for the standard ensembles of random matrices [36, 37]). This property is typically referred to by saying that the spectral form factor is not self-averaging [38]. Moreover, from its definition, we see that $K_g(t)$ with unrestricted trace can be interpreted as the survival probability (or Loshmit echo) for a random initial state, which is another well studied chaos indicator [39, 40].

Note that, if the model is chaotic, at large times the survival probability decays to the number of symmetry sectors.

As mentioned before, here we regard $\mathbb{U}(t)$ as “chaotic” if there exist a scale τ_{th} such that

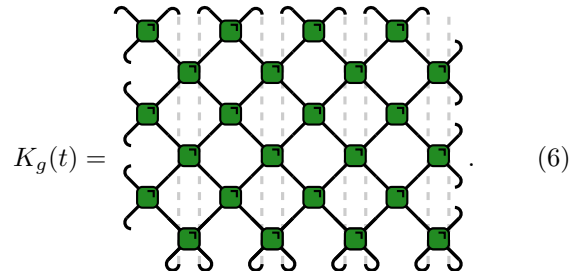
$$K_g(t) \simeq 1 = \mathbb{E}_{\text{CUE}}[|\text{tr} U|^2], \quad \text{for } t \gg \tau_{\text{th}}, \quad (4)$$

where \simeq denotes asymptotic equality in the leading and possibly subleading order in τ_{th}/t . We remark that, since our system is not time-reversal invariant, we considered the average over the circular unitary ensemble (CUE) [36, 41].

To calculate $K_g(t)$ we need to consider two copies of the time evolution operator. Therefore, we “fold” the circuit by placing $\mathbb{U}(t)^\dagger$ on top of $\mathbb{U}(t)$ (see, e.g., Ref. [42]). Introducing the “double gate”

$$W = \text{Diagram of double gate} = \langle \text{Diagram of double gate} \rangle = \langle U_{x,\tau}^\dagger \otimes U_{x,\tau} \rangle, \quad (5)$$

which, after averaging, is assumed to be independent of x, τ , the GSFF is expressed as



$$K_g(t) = \text{Diagram of folded circuit}, \quad (6)$$

Top and bottom lines at the same positions are connected because of the trace.

Following Ref. [42] we consider the case where each gate in the circuit is the same, apart from random 1-qubit gates $e^{i\phi_{x,\tau}\sigma^z}$ (σ^z is the third Pauli matrix) acting as $U(1)$ noise, namely we take the local gates of the form

$$U_{x,\tau} = (e^{i\phi_{x,\tau}\sigma^z} \otimes e^{i\phi_{x+1/2,\tau}\sigma^z}) \cdot U, \quad (7)$$

where U is a fixed $U(4)$ matrix and $\phi_{x,t}$ are independent random variables uniformly distributed over $[-\pi, \pi]$. Next, we perform the average over $\phi_{x,\tau}$ by using

$$\langle e^{i\phi_{x,\tau}\sigma^z} \otimes e^{-i\phi_{x,\tau}\sigma^z} \rangle = \frac{\mathbb{1} \otimes \mathbb{1} + \sigma^z \otimes \sigma^z}{2} \equiv P_z, \quad (8)$$

where the tensor product, unlike in (7), acts on the same site but two copies. From now on, we will only need to consider this *reduced* local operator Hilbert space, since we inserted the projectors in all space-time points. In particular, the local folded Hilbert space is spanned only by diagonal matrices $|\circ\rangle \equiv |\mathbb{1}\rangle$ and $|\bullet\rangle \equiv |\sigma^z\rangle$ instead of $|\circ\rangle \equiv |\mathbb{1}\rangle$ and $|\sigma^{x,y,z}\rangle$ (all Pauli matrices). Therefore, we define a *reduced* folded gate

$$w := (P_z \otimes P_z)W(P_z \otimes P_z) = \text{Diagram of reduced folded gate}, \quad (9)$$

which is the same at each space-time point. Using the most general 4×4 unitary U (cf. (7)) one finds that the reduced gate can be parametrised as

$$w = \begin{pmatrix} 1 & 0 & 0 & 0 \\ 0 & \varepsilon_1 & a & b \\ 0 & c & \varepsilon_2 & d \\ 0 & e & f & g \end{pmatrix}, \quad (10)$$

with 9 real parameters in $[-1, 1]$ and obeying nontrivial constraints, which are equivalent to demanding that w becomes bistochastic after a Hadamard transformation [42].

Let us now express the GSFF after the averaging procedure described above. We start by expanding the trace in the computational basis $\{|e_i^m\rangle\}$ where $m = 0, \dots, 2L$ denotes the particle number (number of quasiparticles \bullet) and $i = 1, \dots, \binom{2L}{m}$ labels states in a fixed m sector. Assuming that there are no conserved charges we have

$$K_g(t) = \sum_{m=0}^{2L} K_g^{(m)}(t) = 1 + K_g^{(1)}(t) + \dots + K_g^{(2L)}(t), \quad (11)$$

where we defined, in ‘1st quantization notation’:

$$K_g^{(m)}(t) \equiv \sum_{\{x_j\}_{j=1}^m}^{x_i > x_j : i > j} \langle \bullet_{x_1} \dots \bullet_{x_m} | \bullet_{x_1} \dots \bullet_{x_m}(t) \rangle_L, \quad (12)$$

and used that $K_g^{(0)}(t) = 1$. We see that $K_g^{(m)}(t)$ is expressed as the sum of the averaged autocorrelation functions of the extended operators $\sigma_{x_1}^z \dots \sigma_{x_m}^z$ (with $x_1 < x_2 < \dots < x_m$, and $x_j \in \mathbb{Z}_{2L}/2$) in finite volume L .

Let us now focus on a special family of reduced gates (10): those with either no *splittings* ($f = e = 0$) or no *mergers* ($b = d = 0$) and with non-negative weights. For this family of gates we can invoke the following property (proven in Sec. I of the Supplemental Material (SM)):

Property 1. *The averaged dynamical correlations $\langle \bullet_{x_1} \dots \bullet_{x_m} | \bullet_{y_1} \dots \bullet_{y_m}(t) \rangle_L$ are upper bounded by*

$$\max \left(1, \frac{g}{\varepsilon_1 \varepsilon_2 + ac} \right)^{(m-1)t} \sum_{\sigma \in S_m} \prod_{i=1}^m \langle \bullet_{x_i} | \bullet_{y_{\sigma(i)}}(t) \rangle_L, \quad (13)$$

where S_m is the permutation group of m elements.

Moreover, we also have:

Property 2. *The two-point functions have the following asymptotic expansion in t*

$$\langle \bullet_x | \bullet_y(t) \rangle_L \simeq \frac{C_{\eta_x, \eta_y}}{C_{0,0} + C_{1,1}} \frac{\lambda^t}{L} + a_{\eta_x}^{2t} \delta_{t-(x-y) \bmod L}, \quad (14)$$

where $\eta_j = 2j \bmod 2$, $\delta_0 = 1$, $\delta_{x \neq 0} = 0$, $a_0 = a$, $a_1 = c$,

$$\lambda = \frac{1}{4} \left((a+c) + \sqrt{4\varepsilon_1 \varepsilon_2 + (a-c)^2} \right)^2 \quad (15)$$

while C_{η_x, η_y} are constant amplitudes ($C_{0,0}$ and $C_{1,1}$ are reported in Sec. II of the SM).

An instructive way to obtain the expansion (14) is to note that the correlations in finite volume can be written as

$$\langle \bullet_x | \bullet_y(t) \rangle_L = \sum_{w=-\lfloor t/L \rfloor}^{\lfloor t/L \rfloor} \langle \bullet_{x+wL} | \bullet_y(t) \rangle_\infty, \quad (16)$$

where $\langle \bullet_x | \bullet_y(t) \rangle_\infty$ are the infinite volume correlations known exactly from Ref. [42]. This form follows from the observation that for no splittings (mergers) the only contributions to the correlation come from continuous paths (the *skeleton diagrams* [42]) connecting the endpoints, and wrapping around the cylindrical worldsheet along the space direction an arbitrary number of times. The maximal number of wrappings is restricted by the maximal speed of propagation. Then, Eq. (14) follows directly plugging in the asymptotic form

$$\langle \bullet_x | \bullet_y(t) \rangle_\infty \simeq \delta_{t-(x-y)} a_{\eta_x}^{2t} + \frac{\lambda^t C_{\eta_x, \eta_y}}{\sqrt{t}} e^{-\frac{(x-y-\bar{\zeta}t)^2}{4Dt}}, \quad (17)$$

[where the diffusion constant is given by $D = [4\pi(C_{0,0} + C_{1,1})^2]^{-1}$ and the fluid velocity $\bar{\zeta}$ is defined in Sec. II] of the SM, and turning the sum over wL/t into an integral for $t \gg L$. Alternatively, Eq. (14) can also be derived by diagonalising an effective Markov operator, see Sec. III of the SM.

Using the asymptotic form (14) for two-point correlations and Property 1 we find (see Sec. IV of the SM)

$$\sum_{m=2}^{2L} K_g^{(m)}(t) < CL^2 \lambda^{2t} \max \left(1, \frac{g^t}{(\varepsilon_1 \varepsilon_2 + ac)^t} \right). \quad (18)$$

This leads us to our **first main result**: for large times and $\lambda \max[1, g/(\varepsilon_1 \varepsilon_2 + ac)] < 1$, the GSFF is fully determined by correlation functions of local observables

$$K_g(t) \simeq 1 + K_g^{(1)}(t) \simeq 1 + \lambda^t + (a^{2t} + c^{2t})L \delta_{t \bmod L}. \quad (19)$$

In particular, since $\lambda > \max(a^2, c^2)$, we find

$$K_g(t) \simeq 1 + e^{-t/\tau_{\text{th}}}, \quad \tau_{\text{th}}^{-1} = -\log \lambda. \quad (20)$$

Note that in this case τ_{th} is the exponent governing the decay of two-point correlations in infinite volume. Note also that there is no L dependence in τ_{th} , in contrast to $\log L$ dependence found in several examples of extended systems, see e.g. [10, 12, 35].

Eq. (19) shows excellent agreement with the exact numerical evaluation of $K_g(t)$, see Fig. 1 for a representative example. Moreover, our numerical observations suggest that the bound (18) is too conservative and Eq. (19) holds whenever $\lambda < 1$, namely whenever the averaged two-point correlations decay exponentially.

When some of the gate’s parameters (10) are negative, the Gaussian asymptotic form (17) is not valid. We calculate $K_g^{(1)}(t) \simeq \lambda^t$ by diagonalising an effective Markov operator, see Sec. III of the SM (λ can be different from the one in (15)). Moreover, we again bound the other

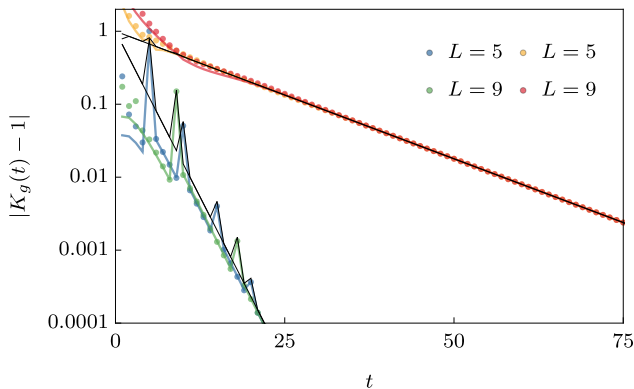


FIG. 1. Deviations of GSFF $K_g(t)$ from the RMT prediction for two different gates with no splittings, $b = d = 0$. Symbols denote the exact numerical results for up to 18 sites ($L = 9$). Solid color line depicts $K_g^{(1)}(t)$ computed according to Eqs. (12) and (16). Notice that the τ_{th} does not scale with L . The solid black lines show the asymptotic from Eq. (19). We wrote the gate's parameters in Table SM-1 of Sec. VI of the SM.

contributions as in (18) (with a minor modification, see Sec. IV of the SM).

Let us now consider a special case for which (18) does not provide a useful bound (because $\lambda = 1$). Namely, the case of averaged gates with a conservation law. This situation can be realised by considering a gate U (and hence $U_{x,\tau}$ in Eq. (7)) that conserves the magnetisation in the z direction and leads to the following averaged gate

$$w_{U(1)} = \begin{pmatrix} 1 & 0 & 0 & 0 \\ 0 & \cos^2 2J & \sin^2 2J & 0 \\ 0 & \sin^2 2J & \cos^2 2J & 0 \\ 0 & 0 & 0 & 1 \end{pmatrix}, \quad J \in [0, \pi/4]. \quad (21)$$

Note that the time-evolution operator generated by this gate is integrable: it is an example of Floquet XXX model at a non-unitary point [43]. Interestingly, a similar Floquet XXX model was obtained in Ref. [13] after averaging a $U(1)$ -symmetric Floquet Haar random circuit. Finally, we remark that a similar reduced gate for driven systems has been studied in Ref. [35].

Since the magnetisation is conserved, the trace in (3) is reduced to a single magnetisation sector. This means that instead of $K_g(t)$ in Eq. (11) we should consider a single term $K_g^{(m)}(t)$ with fixed $m = 0, 1, \dots, 2L$. Moreover, we observe that, apart from the two trivial sectors $m = 0$ and $m = 2L$ where the GSFF is one, all $K_g^{(m)}(t)$ decay to one with the same exponent, see Fig. 2. This can be understood directly from the Bethe-Ansatz solution (see, e.g., the supplemental material of Ref. [13]). Indeed, by looking at the finite volume eigenstates one finds that the lowest excitations (those with eigenvalue of the Markov operator which is the closest to one), are one-magnon excitations (as opposed to bound states or scattering states of many magnons). Since the one-magnon

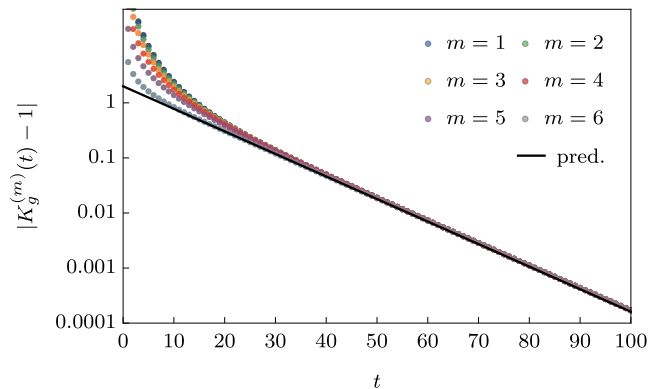


FIG. 2. Deviations of the GSFF $|K_g^{(m)}(t) - 1|$ with conservation laws. We show the results for different magnetisation sectors at $L = 7$ (14 sites) and $J = 0.3$. The black line is the prediction (24).

states are highest weight states of the representation of $SU(2)$ with $S_z = L - 1$, their descendants (obtained by multiple applications of the lowering operators S^-) appear in all sectors $m = 1, \dots, 2L - 1$. Therefore all sectors have the same Thouless time, which can be deduced from the $m = 1$ sector.

For large times, the averaged two-point function for $m = 1$ takes a simple diffusive form

$$\langle \bullet_x | \bullet_0(t) \rangle_\infty \simeq \frac{1}{2\sqrt{4\pi t D}} e^{-\frac{x^2}{4Dt}}, \quad (22)$$

where $D = (\tan^2 2J)/4$ is the diffusion constant and we neglected exponentially small corrections with L -independent exponents because we expect a L -dependent Thouless time. Using again Eq. (16) we have

$$K_g^{(1)}(t) \simeq \frac{1}{2\sqrt{4\pi t D}} \sum_{w=-\lfloor t/L \rfloor}^{\lfloor t/L \rfloor} e^{-\frac{w^2 L^2}{4Dt}}. \quad (23)$$

Extending the summation to $\pm\infty$ [44] and utilising the Poisson summation formula we get

$$K_g^{(1)}(t) \simeq \sum_{n=-\infty}^{\infty} e^{-\frac{4\pi^2 D t n^2}{L^2}} \simeq 1 + 2e^{-t/\tau_{\text{th}}}, \quad \tau_{\text{th}} = \frac{L^2}{4\pi^2 D}. \quad (24)$$

Note that the Thouless time depends on L^2/D , in agreement with previous observations in chaotic systems with diffusive conservation laws [13, 16, 18, 35, 45]. Our derivation gives a straightforward illustration of the origin of this scaling.

Another interesting limiting case is when, in addition to no splittings (or merges), at least one of ε_1 and ε_2 vanishes (note that $\varepsilon_1 = \varepsilon_2 = 0$ if and only if the gate U is dual-unitary [28, 42]). In this case $K_g(t) = 1 + (a^{2t} + c^{2t})L\delta_{t \bmod L} + \dots$, and the GSFF admits a closed-form expression of all orders (see Sec. V of the SM). The model is chaotic when all a, c, g differ

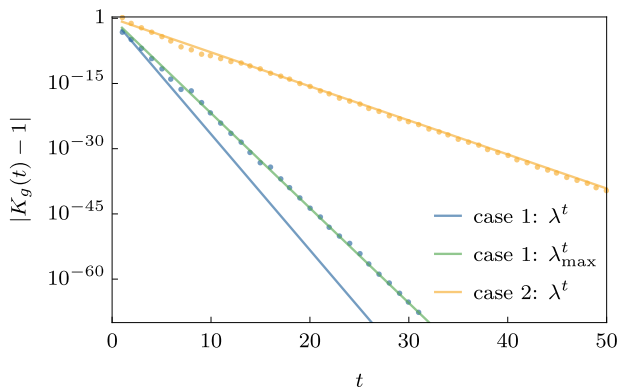


FIG. 3. Symbols show the numerical results for deviations of the spectral form factor $|K(t) - 1|$ with allowed splittings and merges. Solid lines show the decay of the skeleton correlation functions λ^t from (15) and the true decay of the two-point correlation function λ_{\max}^t . In the case 2, the two-point correlation function is well described by the skeleton contributions (see [42] for when this holds). In contrast, the case 1 exhibits a slower decay of the deviations than given by 15, agreeing with the slower decay of the correlation functions. We obtained λ_{\max} from direct numerical evaluation of the two-point correlation functions in infinite volume. The data shown is for the last two gates in Table SM-1 of Sec. VI of the SM, $L = 8$.

from ± 1 . In contrast, if the above conditions do not hold, $K_g(t)$ with unrestricted trace does not decay to the RMT result. This signals new commuting symmetries and possibly non-chaotic behaviour. For instance, for $a = c = g = 1$ (corresponding to the SWAP gate) and unrestricted trace we find $K_g(t)|_{\text{SWAP}} = 4^{\text{gcd}(t,L)}$. Here $\text{gcd}(t, L)$ is the greatest common divisor of L and t . This result is manifestly larger than the RMT result.

In the general case, when both mergers and splittings are allowed, there is a phase transition in the decay exponent of infinite volume correlations [42]. In particular, there is a region in parameter space (see

Eq. (41) in Ref. [42]) where the decay of quasiparticles is still governed by λ in Eq. (15), while for parameters out of this region the exponent changes. Moreover, all $K_g^{(m)}(t)$ will decay with the same exponent (since the number of particles can change during the time evolution, all $K_g^{(m)}(t)$ contain the slow-decaying configurations). However, this means that the decay exponent can again be determined from two-point functions of local operators and that $\tau_{\text{th}} = -1/\log \lambda_{\max}$, where $\lambda_{\max} = \lim_{t \rightarrow \infty} (\max_x \langle \bullet_x | \bullet_0(t) \rangle_{\infty})^{1/t}$. This is in agreement with our numerical experiments, as shown Fig. 3 for a representative example.

In conclusion, we studied the GSFF in a class of local quantum circuits with random longitudinal fields, linking its dynamics with that of (averaged) dynamical correlations of local observables. Specifically, we showed that in the regime where the correlations decay exponentially in time (known as ergodic and mixing in ergodicity theory) the GSFF approaches the prediction of random matrix theory over the same time-scale. Moreover, we proved that the GSFF approaches the prediction of random matrix theory also in the presence of a conservation law, if the correlations take a diffusive form. In this case the timescale is proportional to the system size squared divided by the diffusion constant. Finally, we showed that when the correlations do not decay, the GSFF does not approach the random matrix theory prediction. The correspondence between quantum chaotic and quantum ergodic and mixing regimes is expected on general grounds [40, 46–48] and provides an intuitive understanding of quantum chaos. Our results in a specific setting provide a rigorous proof of such a correspondence. The question of whether our methods can be extended to more general systems sets a direction for further research.

Acknowledgement: The work is supported by the EU Horizon 2020 program through the ERC Advanced Grant OMNES No. 694544, and by the Slovenian Research Agency (ARRS) under the Programme P1-0402. BB was also supported by the Royal Society through the University Research Fellowship No. 201102.

-
- [1] V. I. Arnold and A. Avez, *Ergodic Problems of Classical Mechanics*, Addison-Wesley, Reprint Edition (1989).
 - [2] V. I. Arnold, *Geometrical methods in the theory of ordinary differential equations*, Springer (1988).
 - [3] E. Ott, *Chaos in Dynamical Systems*, 2nd Edition, Cambridge University Press (2012).
 - [4] I. P. Cornfeld, S. V. Fomin, Y. G. Sinai, *Ergodic Theory*, Springer (2012).
 - [5] G. Casati, F. Valz-Gris, and I. Guarneri, *On the connection between quantization of nonintegrable systems and statistical theory of spectra*, *Lett. Nuovo Cimento Soc. Ital. Fis.* **28**, 279 (1980).
 - [6] M. V. Berry, *Quantizing a classically ergodic system: Sinai's billiard and the KKR method*, *Ann. Phys. (N.Y.)* **131**, 163 (1981).
 - [7] O. Bohigas, M. J. Giannoni, and C. Schmit, *Characterization of chaotic quantum spectra and universality of level fluctuation laws*, *Phys. Rev. Lett.* **52**, 1 (1984).
 - [8] P. Hayden and J. Preskill, *Black holes as mirrors: quantum information in random subsystems*, *J. High Energy Phys.* **2007**, 120 (2007).
 - [9] Y. Sekino and L. Susskind, *Fast scramblers*, *J. High Energy Phys.* **2008**, 065 (2008).
 - [10] P. Kos, M. Ljubotina, and T. Prosen, *Many-body quantum chaos: Analytic connection to random matrix theory*, *Phys. Rev. X* **8**, 021062 (2018).
 - [11] A. Chan, A. De Luca, J. T. Chalker, *Solution of a Minimal Model for Many-Body Quantum Chaos*, *Phys. Rev. X* **8**, 041019 (2018).
 - [12] A. Chan, A. De Luca, J. T. Chalker, *Spectral Statistics*

- in Spatially Extended Chaotic Quantum Many-Body Systems, *Phys. Rev. Lett.* **121**, 060601 (2018).
- [13] A. J. Friedman, A. Chan, A. De Luca, J. T. Chalker, *Spectral Statistics and Many-Body Quantum Chaos with Conserved Charge*, *Phys. Rev. Lett.* **123**, 210603 (2019).
- [14] B. Bertini, P. Kos, and T. Prosen, *Exact Spectral Form Factor in a Minimal Model of Many-Body Quantum Chaos*, *Phys. Rev. Lett.* **121**, 264101 (2018).
- [15] S. J. Garratt, J. T. Chalker, *Many-body quantum chaos and the local pairing of Feynman histories*, [arXiv:2008.01697](https://arxiv.org/abs/2008.01697) (2020).
- [16] S. Moudgalya, A. Prem, D. A. Huse, and A. Chan, *Spectral statistics in constrained many-body quantum chaotic systems*, [arXiv:2009.11863](https://arxiv.org/abs/2009.11863) (2020).
- [17] A. Keselman, L. Nie, and E. Berg, *Scrambling and Lyapunov Exponent in Unitary Networks with Tunable Interactions*, [arXiv:2009.10104](https://arxiv.org/abs/2009.10104) (2020).
- [18] D. Roy and T. Prosen, *Random Matrix Spectral Form Factor in Kicked Interacting Fermionic Chains*, [arXiv:2005.10489](https://arxiv.org/abs/2005.10489) (2020).
- [19] B. Bertini, P. Kos, and T. Prosen, *Operator Entanglement in Local Quantum Circuits I: Chaotic Dual-Unitary Circuits*, *SciPost Phys.* **8**, 067 (2020).
- [20] B. Bertini, P. Kos, and T. Prosen, *Operator Entanglement in Local Quantum Circuits II: Solitons in Chains of Qubits*, *SciPost Phys.* **8**, 068 (2020).
- [21] P. W. Claeys and A. Lamacraft, *Maximum velocity quantum circuits*, [arXiv:2003.01133](https://arxiv.org/abs/2003.01133) (2020).
- [22] V. Alba, J. Dubail, and M. Medenjak, *Operator Entanglement in Interacting Integrable Quantum Systems: The Case of the Rule 54 Chain*, *Phys. Rev. Lett.* **122**, 250603 (2019).
- [23] C. Jonay, D. A. Huse, A. Nahum, *Coarse-grained dynamics of operator and state entanglement*, [arXiv:1803.00089](https://arxiv.org/abs/1803.00089) (2018).
- [24] B. Bertini and L. Piroli, *Scrambling in Random Unitary Circuits: Exact Results*, *Phys. Rev. B* **102**, 064305 (2020).
- [25] A. Nahum, S. Vijay, and J. Haah, *Operator Spreading in Random Unitary Circuits*, *Phys. Rev. X* **8**, 021014 (2018).
- [26] C. W. von Keyserlingk, T. Rakovszky, F. Pollmann, and S. L. Sondhi, *Operator Hydrodynamics, OTOCs, and Entanglement Growth in Systems without Conservation Laws*, *Phys. Rev. X* **8**, 021013 (2018).
- [27] A. Nahum, J. Ruhman, S. Vijay, and J. Haah, *Quantum Entanglement Growth under Random Unitary Dynamics*, *Phys. Rev. X* **7**, 031016 (2017).
- [28] B. Bertini, P. Kos, and T. Prosen, *Exact Correlation Functions for Dual-Unitary Lattice Models in 1 + 1 Dimensions*, *Phys. Rev. Lett.* **123**, 210601 (2019).
- [29] S. H. Shenker and D. Stanford, *Black holes and the butterfly effect*, *J. High Energy Phys.* **2014**, 67 (2014).
- [30] D. A. Roberts, D. Stanford, and L. Susskind, *Localized shocks*, *J. High Energy Phys.* **2015**, 51 (2015).
- [31] J. Maldacena, S. H. Shenker, and D. Stanford, *A bound on chaos*, *J. High Energy Phys.* **2016**, 106 (2016).
- [32] T. Prosen and M. Žnidarič, *Is the efficiency of classical simulations of quantum dynamics related to integrability?*, *Phys. Rev. E* **75**, 015202 (2007).
- [33] P. Hosur, X.-L. Qi, D. A. Roberts, and B. Yoshida, *Chaos in quantum channels*, *J. High Energy Phys.* **2016**, 4 (2016).
- [34] P. Saad, S. H. Shenker, and D. Stanford, *A semiclassical ramp in SYK and in gravity*, [arXiv:1806.06840](https://arxiv.org/abs/1806.06840) (2020).
- [35] H. Gharibyan, M. Hanada, S. H. Shenker, and M. Tezuka, *Onset of random matrix behavior in scrambling systems*, *J. High Energy Phys.* **2018**, 124 (2018).
- [36] F. Haake, *Quantum Signatures of Chaos*, 2nd ed. (Springer, 2001).
- [37] H. Kunz, *The probability distribution of the spectral form factor in random matrix theory*, *J. Phys. A: Math. Gen.* **32**, 2171 (1999).
- [38] R. Prange, *The Spectral Form Factor Is Not Self-Averaging*, *Phys. Rev. Lett.* **78**, 2280 (1997).
- [39] E. J. Torres-Herrera and L. F. Santos, *Dynamical manifestations of quantum chaos: correlation hole and bulge*, *Phil. Trans. R. Soc. A.* **375**: 20160434 (2017).
- [40] T. Gorin, T. Prosen, T. H. Seligman and M. Žnidarič, *Dynamics of Loschmidt echoes and fidelity decay*, *Phys. Rep.* **435**, 33 (2006).
- [41] M. L. Mehta, *Random Matrices and the Statistical Theory of Spectra*, 2nd ed. (Academic, New York, 1991).
- [42] P. Kos, B. Bertini and T. Prosen, *Correlations in Perturbed Dual-Unitary Circuits: Efficient Path-Integral Formula*, [arXiv:2006.07304](https://arxiv.org/abs/2006.07304) (2020).
- [43] M. Vanicat, L. Zadnik, and T. Prosen, *Integrable Trotterization: Local Conservation Laws and Boundary Driving*, *Phys. Rev. Lett.* **121**, 030606 (2018).
- [44] It can be done up to exponential corrections with L -independent characteristic time.
- [45] J. Šuntajs, J. Bonča, T. Prosen, and L. Vidmar, *Quantum chaos challenges many-body localization*, [arXiv:1905.06345](https://arxiv.org/abs/1905.06345) (2019).
- [46] T. Prosen, *Chaos and complexity of quantum motion*, *J. Phys. A* **40**, 7881 (2007).
- [47] M. Degli Esposti, S. Graffi, and S. Isola, *Classical limit of the quantized hyperbolic toral automorphisms*, *Commun. Math. Phys.* **167**, 471 (1995).
- [48] G. Casati and B. V. Chirikov, eds., *Quantum chaos between order and disorder*, (Cambridge University Press, Cambridge 1995).
- [49] ITensor Library (version 3), <http://itensor.org>

Supplemental Material for “Chaos and Ergodicity in Extended Quantum Systems with Noisy Driving”

Here we report some useful information complementing the main text. In particular

- In Section I we prove Property 1;
- In Section II we compute the asymptotics of the averaged two-point functions of local operators in infinite volume;
- In Section III we compute $K_g^{(1)}(t)$ using an effective Markov operator;
- In Section IV we establish the bound in Eq. (18);
- In Section V we compute $K_g(t)$ with unrestricted trace for $f = e = \varepsilon_1 = 0$;
- In Section VI we report the parameters of the gates used in our numerical experiments;

I. PROOF OF PROPERTY 1

In this appendix we prove Property 1, namely we show that for no splittings $e = f = 0$ (or no mergers $b = d = 0$) and non-negative weights the $2m$ -point correlation functions $\langle \bullet_{x_1} \cdots \bullet_{x_m} | \bullet_{y_1} \cdots \bullet_{y_m}(t) \rangle_L$ are bounded by

$$\langle \bullet_{x_1} \cdots \bullet_{x_m} | \bullet_{y_1} \cdots \bullet_{y_m}(t) \rangle_L < \left(\max\left(1, \frac{g}{\varepsilon_1 \varepsilon_2 + ac}\right) \right)^{(m-1)t} \sum_{\sigma \in S_m} \prod_{i=1}^m \langle \bullet_{x_i} | \bullet_{y_{\sigma(i)}}(t) \rangle_L, \quad (\text{SM-1})$$

where S_m is the permutation group of m elements.

We start by expressing the correlation functions as the sum of contributions from allowed configurations, as discussed in Section V A of [42]. Inserting a resolution of the identity $\mathbb{1} = |\circ\rangle\langle\circ| + |\bullet\rangle\langle\bullet|$ at each reduced-operator wire, we can explicitly decompose each

$$\langle \bullet_{x_1} \cdots \bullet_{x_m} | \bullet_{y_1} \cdots \bullet_{y_m}(t) \rangle_L = \text{Diagram}, \quad (\text{SM-2})$$

into the sum of 2^{4Lt} terms. Configurations are expressed in terms of “tiles” where we connect the particles \bullet with solid lines and ignore the vacancies \circ [42]. For example,

$$g = \text{Diagram} = \text{Diagram}, \quad (\text{SM-3})$$

The complete set of allowed tiles (corresponding to non-zero coefficients of the gate (10)), when there are no splittings or mergers, is given by:

$$\begin{aligned} \text{Diagram} &= 1 & \text{Diagram} &= a & \text{Diagram} &= c \\ \text{Diagram} &= \varepsilon_1 & \text{Diagram} &= \varepsilon_2 & \text{Diagram} &= g \end{aligned} \quad (\text{SM-4})$$

Note that, if there are no splittings(mergers), and we need to end up with the same number of \bullet , we can not have any mergers(splittings). We start with $m = 2$. The four-point correlation function can be expressed as the sum of the weights of configurations C_i^4

$$\langle \bullet_{x_1} \bullet_{x_2} | \bullet_{y_1} \bullet_{y_2}(t) \rangle_L = \sum_i w(C_i^4), \quad (\text{SM-5})$$

where configurations C_i^4 have four fixed boundary conditions at $x_1, x_2; y_1, y_2$. For example:

$$C_e^4 = \begin{array}{c} \text{Diagram of a diamond-shaped grid with a path of thick black lines} \end{array}, \quad (\text{SM-6})$$

where $x_1 = y_1 = 3/2$ and $x_2 = y_2 = 5/2$. The $w(C)$ is the weight of the configuration, which is a product of the weights of all tiles. For instance, the weight of the tile $w(g \text{ tile}) = g$ and $w(C_e^4) = gac\varepsilon_1^2\varepsilon_2^2$.

Next, we define a map \mathcal{F} , which maps configuration to a set of configurations

$$\mathcal{F}(C_i^4) = \{\tilde{C}_{i,k}^4\}_{k=1}^{2^n}, \quad (\text{SM-7})$$

where n is the number of g tiles in C_i^4 . It maps each tile g to either tile ac or tile $\varepsilon_1\varepsilon_2$ resulting in 2^n different configurations

$$\mathcal{F}(\text{diamond with } g \text{ tile}) = \left\{ \text{diamond with } ac \text{ tile}, \text{ diamond with } \varepsilon_1\varepsilon_2 \text{ tile} \right\}. \quad (\text{SM-8})$$

Configurations denoted by tilde $\tilde{}$ have “new tiles” ac and $\varepsilon_1\varepsilon_2$ and no g tiles.

$$\mathcal{F}(C_e^4) = \left\{ \begin{array}{c} \text{Diagram 1: Original path with } g \text{ tiles replaced by } ac \text{ tiles} \\ \text{Diagram 2: Original path with } g \text{ tiles replaced by } \varepsilon_1\varepsilon_2 \text{ tiles} \end{array} \right\}. \quad (\text{SM-9})$$

For this map we can prove the following

Lemma 1. \mathcal{F} is surjective, namely $\mathcal{F}(x) \cap \mathcal{F}(y) = \{\}$, for $x \neq y$.

Proof. Since $x \neq y$, the configurations differ in at least one tile. Moreover, because a tile g is the only tile with two incoming lines, they need to differ in a tile different from g . \mathcal{F} does not change tiles different from g , therefore the resulting configurations from different configurations differ in the initially different tile. The configurations from the same set are different by construction. \square

Next, notice that we can express the sum of the weights of tilde configurations with weights of configurations without the tilde

$$\sum_{k=1}^{2^n} w(\tilde{C}_{i,k}^4) = \left(\frac{\varepsilon_1\varepsilon_2 + ac}{g} \right)^n w(C_i^4), \quad (\text{SM-10})$$

where we used the factorisation of the weights. To see that, notice that we can factor out from the sum the weights of all tiles different from g in C_i and tiles at the same positions in tilde configurations. Then we are left only with a product of g tiles, with each of them mapped to $(\varepsilon_1\varepsilon_2 + ac)$.

For instance, a configuration with of two g tiles

$$w(C_i^4) = gg \quad (\text{SM-11})$$

maps to

$$\sum_{k=1}^4 w(\tilde{C}_{i,k}^4) = (\varepsilon_1\varepsilon_2 + ac)(\varepsilon_1\varepsilon_2 + ac). \quad (\text{SM-12})$$

Since each tiling $\tilde{C}_{i,k}^4$ is different and corresponds to a different term in the diagrams of $(\langle \bullet_{x_1} | \bullet_{y_1}(t) \rangle_L \langle \bullet_{x_2} | \bullet_{y_2}(t) \rangle_L + \langle \bullet_{x_1} | \bullet_{y_2}(t) \rangle_L \langle \bullet_{x_2} | \bullet_{y_1}(t) \rangle_L)$, it follows that

$$\sum_i \sum_{k=1}^{2^n} w(\tilde{C}_{i,k}^4) \leq (\langle \bullet_{x_1} | \bullet_{y_1}(t) \rangle_L \langle \bullet_{x_2} | \bullet_{y_2}(t) \rangle_L + \langle \bullet_{x_1} | \bullet_{y_2}(t) \rangle_L \langle \bullet_{x_2} | \bullet_{y_1}(t) \rangle_L). \quad (\text{SM-13})$$

Finally, using that the maximal possible number of g tiles is t (for $L > 1$), we see

$$\langle \bullet_{x_1} \bullet_{x_2} | \bullet_{y_1} \bullet_{y_2}(t) \rangle_L \leq \left[\max \left(1, \frac{g^t}{(\varepsilon_1 \varepsilon_2 + ac)^t} \right) \right] (\langle \bullet_{x_1} | \bullet_{y_1}(t) \rangle_L \langle \bullet_{x_2} | \bullet_{y_2}(t) \rangle_L + \langle \bullet_{x_1} | \bullet_{y_2}(t) \rangle_L \langle \bullet_{x_2} | \bullet_{y_1}(t) \rangle_L). \quad (\text{SM-14})$$

Similarly, for $2 < m < 2L$ we use that the maximal possible number of g tiles is $(m-1)t$ to find (SM-1).

II. ASYMPTOTICS OF INFINITE-VOLUME CORRELATION FUNCTIONS

1. Asymptotics between integer indexed points

Let us start considering the correlation functions between integer indexed points. First we note that they can be expressed in terms of the ordinary hypergeometric function and the Jacobi polynomials.

$$\begin{aligned} \langle \bullet_x | \bullet_0(t) \rangle_\infty &= \sum_{n=1}^t \left(\frac{\varepsilon_1 \varepsilon_2}{ac} \right)^n \binom{t+x}{n} \binom{t-x-1}{n-1} a^{t+x} c^{t-x} + \delta_{t,x} a^{2t} \\ &= a^{t+x} c^{t-x} \frac{\varepsilon_1 \varepsilon_2 (t+x)}{ac} {}_2F_1 \left(1-t-x, 1-t+x; 2; \frac{\varepsilon_1 \varepsilon_2}{ac} \right) + \delta_{t,x} a^{2t}, \end{aligned} \quad (\text{SM-15})$$

where ${}_2F_1$ is Gaussian or ordinary hypergeometric function. The expression can be expressed using Jacobi polynomials $P_n^{(\alpha, \beta)}$ as

$$\langle \bullet_x | \bullet_0(t) \rangle_\infty = a^{t+x} c^{t-x} z P_{t+x-1}^{(1, -2t)}(1-2z) + \delta_{t,x} a^{2t}, \quad (\text{SM-16})$$

where we introduced $z = \varepsilon_1 \varepsilon_2 / ac$.

We now proceed to develop the asymptotic expansion of (SM-15). We begin by writing it in terms of the ray variable $\zeta = x/t \in [-1, 1]$

$$\langle \bullet_{\zeta t} | \bullet_0(t) \rangle_\infty = \delta_{\zeta-1} a^{2t} + \sum_{n=1}^{\min(t(1+\zeta), t(1-\zeta))} P_n(\zeta, t), \quad (\text{SM-17})$$

with

$$P_n(\zeta, t) = z^n \binom{t(1+\zeta)}{n} \binom{t(1-\zeta)-1}{n-1} a^{t(1+\zeta)} c^{t(1-\zeta)}, \quad (\text{SM-18})$$

and $z = \varepsilon_1 \varepsilon_2 / ac$. We obtain the asymptotic form by firstly using the Stirling's approximation for P_n . Then we write the Taylor expansion for $\log P_n$ in n around the maximum, substitute the sum over n by the integral and integrate over n . Finally, we write the Taylor expansion for $\log \langle \bullet_{\zeta t} | \bullet_0(t) \rangle_\infty$ in terms of ζ to second order around the maximum. Therefore, we obtain Gaussian form of the correlations, which accurately describes the asymptotic behaviour.

Stirling's approximation for P_n yields

$$P_n(\zeta, t) \approx z^n a^{t(1+\zeta)} c^{t(1-\zeta)} \sqrt{\frac{t^2(1-\zeta^2) - t(1+\zeta)}{(2\pi)^2(n^2-n)((t-n)^2 - (t\zeta)^2)}} \frac{(t(1+\zeta))^{t(1+\zeta)} (t(1-\zeta)-1)^{t(1-\zeta)-1}}{n^n (n-1)^{n-1} (t(1+\zeta)-n)^{t(1+\zeta)-n} (t(1-\zeta)-n)^{t(1-\zeta)-n}}. \quad (\text{SM-19})$$

Next we find the maximum \bar{n} , by demanding that the derivative of $\log P_n(\zeta, t)$ vanishes. We obtain the equation

$$\log \frac{z(t(1+\zeta) - \bar{n})(t(1-\zeta) - \bar{n})}{\bar{n}(\bar{n}-1)} = -\frac{1}{2} \left(\frac{1}{\zeta t - \bar{n} + t} + \frac{1}{-\zeta t - \bar{n} + t} + \frac{1-2\bar{n}}{(\bar{n}-1)\bar{n}} \right), \quad (\text{SM-20})$$

which we solve up to $1/t$ order. We obtain

$$\bar{n} = vt + n_0 + \mathcal{O}(1/t), \quad v = \frac{z - \sqrt{z + \zeta^2(z^2 - z)}}{z - 1}, \quad (\text{SM-21})$$

where we took the relevant root of the quadratic equation, for which $0 \geq v \geq 1$. The expression for n_0 contains the first sub-leading terms from LHS of Eq. (SM-20) and the leading order from RHS.

$$n_0 = \frac{1}{2} \frac{v^2 - v}{v + \zeta^2 - 1} = \frac{1}{2} \frac{z + \zeta^2(z^2 - z) - \sqrt{z + \zeta^2(z^2 - z)}}{z - 1 + \zeta^2(z - 1)^2}. \quad (\text{SM-22})$$

Next, we derive $S_{\bar{n}} = -\frac{\partial^2 \log P_{\bar{n}}}{\partial \bar{n}^2} |_{\bar{n}}$

$$S_{\bar{n}} = \frac{2z}{v^3 t} (1 - v - \zeta^2). \quad (\text{SM-23})$$

The simplified value at the saddle point $P_{\bar{n}}(\zeta, t)$ reads

$$P_{\bar{n}}(\zeta, t) = \frac{\sqrt{z}}{2\pi v t} \sqrt{\frac{1 + \zeta}{1 - \zeta}} \left[acz \frac{1 - \zeta^2}{v^2} \left(\frac{a(1 + \zeta)(1 - \zeta - v)}{c(1 - \zeta)(1 + \zeta - v)} \right)^\zeta \right]^t. \quad (\text{SM-24})$$

Next, we approximate the sum with the integral and obtain

$$\langle \bullet_{\zeta t} | \bullet_0(t) \rangle_\infty = \delta_{\zeta-1} a^{2t} + \int_0^t dn P_{\bar{n}}(\zeta, t) e^{-S_{\bar{n}}(n - \bar{n})^2/2} = \delta_{\zeta-1} a^{2t} + \sqrt{2\pi/S_{\bar{n}}} P_{\bar{n}}(\zeta, t). \quad (\text{SM-25})$$

The asymptotic form is:

$$\langle \bullet_{\zeta t} | \bullet_0(t) \rangle_\infty = \delta_{\zeta-1} a^{2t} + \frac{1}{2} \sqrt{\frac{v}{\pi t} \frac{(1 + \zeta)}{(1 - \zeta)(1 - v - \zeta^2)}} \left[acz \frac{1 - \zeta^2}{v^2} \left(\frac{a(1 + \zeta)(1 - \zeta - v)}{c(1 - \zeta)(1 + \zeta - v)} \right)^\zeta \right]^t. \quad (\text{SM-26})$$

The expression is rather involved, but it is well approximated by a Gaussian function of ζ . To find it we first determine the maximum versus ζ . Taking the first derivative equal to 0 leads to

$$\bar{\zeta} = \zeta_0 + \frac{1}{t} \zeta_1 + \mathcal{O}(1/t^2), \quad \zeta_0 = \frac{a - c}{\sqrt{(a - c)^2 + 4acz}} = \frac{a - c}{\Delta}. \quad (\text{SM-27})$$

We introduced $\Delta = \sqrt{4acz + (a - c)^2}$. To get the correct normalization of the final result, we need to obtain the $\mathcal{O}(1/t)$ term. It reads

$$\zeta_1 = \frac{\Delta (a^2 c(20z - 11) + 3a^3 + 3ac^2(4z - 1) + 3c^3) + 2ac(z - 1)(a - c)(a + c)}{2(4acz + (a - c)^2)(3a^2 + 2ac(8z - 5) + 3c^2)}. \quad (\text{SM-28})$$

The second derivative at $\bar{\zeta}$ up to first order

$$S_{\bar{\zeta}} = \frac{((a - c)^2 + 4acz)^{3/2}}{2acz|a + c|} = \frac{\Delta^3}{2acz|a + c|}. \quad (\text{SM-29})$$

We obtain the final form

$$\langle \bullet_{\zeta t} | \bullet_0(t) \rangle_\infty = \delta_{\zeta-1} a^{2t} + \frac{C_{0,0}}{\sqrt{t}} \lambda^t e^{-t S_{\bar{\zeta}} (\zeta - \bar{\zeta})^2/2}, \quad (\text{SM-30})$$

with

$$\lambda = \frac{1}{4} \left((a + c) + \sqrt{4acz + (a - c)^2} \right)^2. \quad (\text{SM-31})$$

and

$$C_{0,0} = \frac{1}{2} \sqrt{\frac{v_0}{\pi} \frac{(1 + \zeta_0)}{(1 - \zeta_0)(1 - v_0 - \zeta_0^2)}} \times \left(\frac{a \left(\zeta_0 \left(\zeta_0 + 2\sqrt{\zeta_0^2(z - 1)z + z - 2\zeta_0 z} \right) - 1 \right)}{c(\zeta_0^2 - 1)} \right)^{\zeta_1}, \quad (\text{SM-32})$$

with $v_0 = v(\zeta_0)$. A comparison with the exact evaluation is shown in Fig. SM-1.

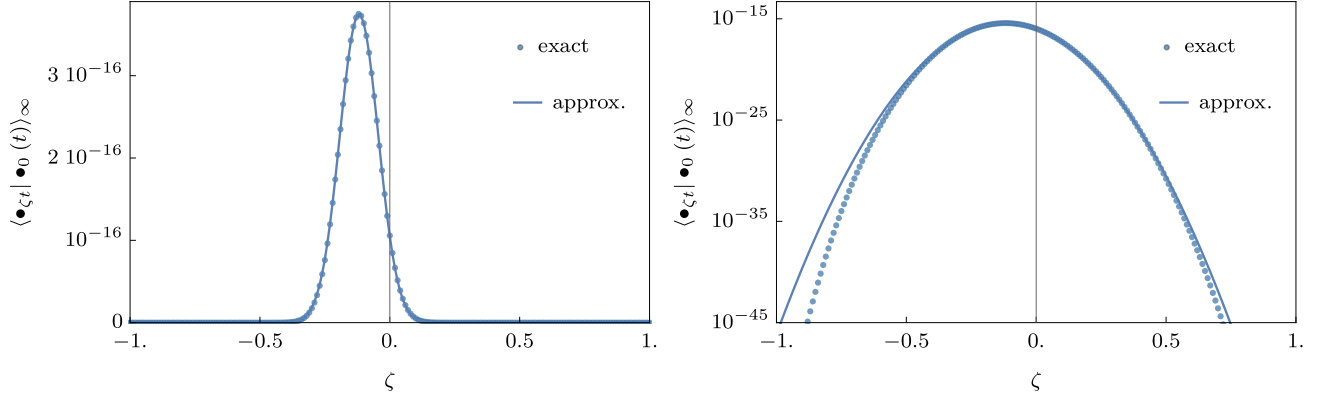


FIG. SM-1. Comparison between asymptotic formula (SM-30) and exact evaluation (SM-15). $t = 100$, $a = 0.4$, $c = 0.5$ and $z = 0.8$.

2. Asymptotics between integer and half-integer indexed points

The calculation of the asymptotics for correlations with different endpoints follows the same lines. The final results read as

$$\langle \bullet_{x+1/2} | \bullet_{1/2}(t) \rangle_{\infty} = \delta_{\zeta+1} c^{2t} + \frac{C_{1,1}}{\sqrt{t}} \lambda^t e^{-tS_{\zeta}(\zeta-\bar{\zeta})^2/2}, \quad (\text{SM-33})$$

$$\langle \bullet_{x+1/2} | \bullet_0(t) \rangle_{\infty} = \frac{C_{0,1}}{\sqrt{t}} \lambda^t e^{-tS_{\zeta}(\zeta-\bar{\zeta})^2/2}, \quad (\text{SM-34})$$

$$\langle \bullet_x | \bullet_{1/2}(t) \rangle_{\infty} = \frac{C_{1,0}}{\sqrt{t}} \lambda^t e^{-tS_{\zeta}(\zeta-\bar{\zeta})^2/2}, \quad (\text{SM-35})$$

where $x \in \mathbb{Z}_L$, $C_{1,1} = \sqrt{\frac{S_{\bar{\zeta}}}{2\pi}} - C_{0,0}$, and we do not report an explicit form of $C_{1,0}$ and $C_{0,1}$ as it is not needed in the main text.

III. EFFECTIVE MARKOV MATRIX FOR THE $m = 1$ SECTOR

We begin by noting that $K_g^{(1)}(t)$ can be written as the trace of the following $2L \times 2L$ block-circulant Markov operator

$$\mathbb{M} = \begin{pmatrix} A & B & 0 & 0 & \dots & 0 & C \\ C & A & B & 0 & \dots & 0 & 0 \\ 0 & C & A & B & \dots & 0 & 0 \\ \vdots & & & & \ddots & & \vdots \\ B & 0 & 0 & 0 & \dots & C & A \end{pmatrix}, \quad (\text{SM-36})$$

where we introduced the following 2×2 matrices

$$A = \begin{pmatrix} \varepsilon_1 \varepsilon_2 & c \varepsilon_2 \\ a \varepsilon_1 & \varepsilon_1 \varepsilon_2 \end{pmatrix}, \quad B = \begin{pmatrix} c^2 & 0 \\ c \varepsilon_1 & 0 \end{pmatrix}, \quad C = \begin{pmatrix} 0 & a \varepsilon_2 \\ 0 & a^2 \end{pmatrix}. \quad (\text{SM-37})$$

The eigenvectors of \mathbb{M} can then be written as

$$w_m^{\pm} = \begin{pmatrix} v_m^{\pm} \\ e^{i \frac{2\pi m}{L}} v_m^{\pm} \\ \vdots \\ e^{i \frac{2\pi m}{L} (L-1)} v_m^{\pm} \end{pmatrix}, \quad m = 0, \dots, L-1, \quad (\text{SM-38})$$

where v_m^\pm are the two eigenvectors of

$$A + e^{i\frac{2\pi m}{L}} B + e^{-i\frac{2\pi m}{L}} C. \quad (\text{SM-39})$$

The eigenvalues are given by

$$\lambda_m^\pm = \frac{1}{4} \left((ae^{-\frac{i\pi m}{L}} + ce^{\frac{i\pi m}{L}}) \pm \sqrt{(ae^{-\frac{i\pi m}{L}} - ce^{\frac{i\pi m}{L}})^2 + 4\varepsilon_1\varepsilon_2} \right)^2. \quad (\text{SM-40})$$

In particular, the eigenvalue with largest absolute magnitude is one of the four choices:

$$\lambda_0^\pm = \frac{1}{4} \left(a + c \pm \sqrt{(a-c)^2 + 4\varepsilon_1\varepsilon_2} \right)^2, \quad \lambda_{L/2}^\pm = -\frac{1}{4} \left(a - c \pm \sqrt{(a+c)^2 - 4\varepsilon_1\varepsilon_2} \right)^2. \quad (\text{SM-41})$$

λ_0^+ is the relevant solution when all parameters are positive, and coincides with λ in Eq. (15) of the main text. In this case we immediately get

$$K_g^{(1)}(t) = \text{tr} [\mathbb{M}^t] \simeq (\lambda_0^+)^t. \quad (\text{SM-42})$$

IV. BOUND ON $K_g^{(m)}(t)$

In this appendix we use Property 1 and Eq. (14) to find a bound for

$$K_g^{(2+)}(t) \equiv \sum_{m=2}^{2L} K_g^{(m)}(t). \quad (\text{SM-43})$$

Summing the

$$\binom{2L}{m} \leq \frac{(2L)^m}{m!} \quad (\text{SM-44})$$

m -point correlation functions in $K_g^{(m)}$ for $1 < m < 2L$ we get

$$K_g^{(m)} < G(2L)^m \lambda^{mt} \left(\max \left(1, \frac{g^{(m-1)t}}{(\varepsilon_1\varepsilon_2 + ac)^{(m-1)t}} \right) \right), \quad (\text{SM-45})$$

where G is a constant. For the sector with $m = 2L$ we instead find exactly $K_g^{(2L)}(t) = g^{4Lt}$. Combining the bounds for all terms (SM-45), we obtain

$$K_g^{(2+)}(t) < G\gamma^2 \frac{1}{1-\gamma} \left(\max \left(1, \frac{g}{\varepsilon_1\varepsilon_2 + ac} \right) \right)^{-t}, \quad (\text{SM-46})$$

with

$$\gamma = 2L\lambda^t \left(\max \left(1, \frac{g^t}{(\varepsilon_1\varepsilon_2 + ac)^t} \right) \right). \quad (\text{SM-47})$$

This is much smaller than $K_1(t)$ for $\lambda \max[1, g/(\varepsilon_1\varepsilon_2 + ac)] < 1$. Empirically, this condition seems to hold in 83% of randomly generated gates with no splittings and positive weights. We compare the bound with a numerical evaluation of $K_g^{(2+)}(t)$ in Fig SM-2.

A. Bound on $K_g^{(m)}(t)$ in the case of negative weights

For gates with negative weights we have $K_g^{(1)} \simeq \lambda_1^t$, where λ_1 is the largest in the magnitude of the eigenvalues in (SM-41). On the other hand, the two-point correlation function at long times are bounded from above by the

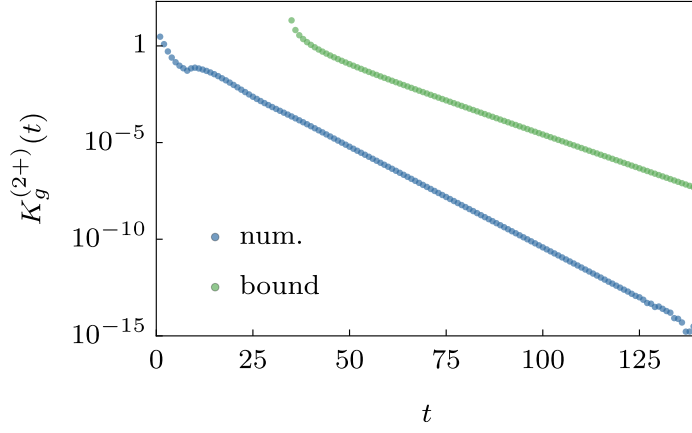


FIG. SM-2. Exact numerical evaluation of $K_g^{(2+)}(t)$ vs bound SM-49 (for $G = 1$). We see that $K_g^{(2+)}(t)$ the bound is not tight. Here we took $L = 8$, and the gate's parameters are given in the second row of Tab. SM-1.

asymptotic form for the effective gate, where the parameters of the gate are substituted by their absolute values. In particular, we have

$$\lambda_{\text{eff}} = \frac{1}{4} \left(|a| + |c| + \sqrt{(|a| - |c|)^2 + 4|\varepsilon_1||\varepsilon_2|} \right)^2. \quad (\text{SM-48})$$

Thus, we get

$$K_g^{(2+)}(t) < G\gamma^2 \frac{1}{1-\gamma} \left(\max \left(1, \frac{|g|}{|\varepsilon_1||\varepsilon_2| + |a||c|} \right) \right)^{-1}, \quad (\text{SM-49})$$

with

$$\gamma = 2L\lambda_{\text{eff}}^t \left(\max \left(1, \frac{|g|^t}{(|\varepsilon_1||\varepsilon_2| + |a||c|)^t} \right) \right). \quad (\text{SM-50})$$

We see that $K_g^{(2+)}(t)$ is certainly exponentially smaller than $K_g^{(1)}(t)$ for

$$\frac{\lambda_{\text{eff}}^2}{|\lambda_1|} \max \left(1, \frac{|g|}{|\varepsilon_1||\varepsilon_2| + |a||c|} \right) < 1, \quad (\text{SM-51})$$

which holds in 90% of randomly generated gates with no splittings and at least one of $a, c, \varepsilon_1, \varepsilon_2, g$ negative.

V. $K_g(t)$ FOR $f = e = \varepsilon_1 = 0$

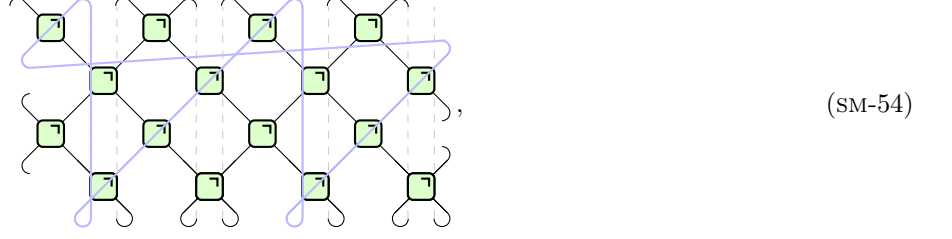
Here it is more convenient to look at the following representation ($L = 4, t = 2$)

$$K_g(t) = \begin{array}{c} \text{Diagram of a 4x4 grid of green squares with black lines representing gates. The diagram is labeled (SM-52).} \end{array} \quad (\text{SM-52})$$

Since we do not allow splittings ($e = f = 0$) the merges will not appear in the evaluation of (SM-52). Otherwise there would be a different number of operators at the bottom and the top. Furthermore, since $\varepsilon_1 = 0$, we cannot convert left mover to right mover. Since the number of right movers at the bottom and the top is the same, also $\varepsilon_2 = 0$. Therefore, the only allowed tiles are (see discussion around (SM-3) for the introduction of tiles)

$$\begin{array}{c} \text{Diagram showing four types of green diamond tiles: 1. Empty diamond = 1; 2. Diamond with diagonal line from top-left to bottom-right = a; 3. Diamond with diagonal line from top-right to bottom-left = c; 4. Diamond with both diagonals = g. The diagram is labeled (SM-53).} \end{array} \quad (\text{SM-53})$$

We start by considering \bullet on a site and follow the evolution of a state on a single wire until the line closes on itself, which we call an *orbit*. For example



(SM-54)

where we used periodic boundary conditions in space and time (from trace). The state on a given wire travels straight along the light-cone. When it reaches the top, the trace acts as a periodic boundary condition in time. Therefore it continues to travel until it reaches the starting point. When it reaches the starting point, it has traveled through 2ℓ gates, with $\ell = \text{lcm}(t, L)$ (lcm stands for least common multiplier). There are $o = tL/\ell$ of distinct left(right)-moving orbits. Each orbit can either be occupied by the operator \circ or \bullet , which has weights 1 or $c^{2\ell}$ ($a^{2\ell}$ for right moving orbits), respectively.

Consider first the case $g = 0$. Here, we can have only left or right moving orbits filled with \bullet , or else they cross and contribute 0. Therefore

$$K_g(t) = 1 + \sum_{n=1}^o \binom{o}{n} (a^{2n\ell} + c^{2n\ell}) = (1 + a^{2\ell})^o + (1 + c^{2\ell})^o - 1, \quad (\text{SM-55})$$

where n counts the number of orbits occupied by \bullet .

In case $g \neq 0$, left and right moving orbits are allowed to cross, and we need to count the number of crossings and the combinatorial factors. The orbits cross $\binom{n}{o} \binom{m}{o} 2tL$ times, where n and m are the number of right and left moving orbits filled with \bullet , respectively. Putting it all together, we find

$$K_g(t) = \sum_{n,m=0}^{tL/\ell} \binom{tL/\ell}{n} \binom{tL/\ell}{m} a^{2n\ell} c^{2m\ell} \left[\frac{g}{ac} \right]^{2\ell^2 nm/tL}. \quad (\text{SM-56})$$

VI. NUMERICAL METHODS AND PARAMETERS OF THE GATES

Direct numerical evaluations have been performed by exactly computing $K(t)$. We achieved that by exactly contracting the diagram (SM-52), using some basic functionalities of ITensor Library [49]. The parameters of the gates used in numerical experiments are given in Table SM-1.

	a	b	c	d	e	f	g	ε_1	ε_2
Gate red/yellow	0.761132	0	0.761132	0	-0.025732	-0.025732	0.701678	0.05	0.05
Gate green/blue	.5	0	0.7	0	0	0	0.25	0.3	0.4
Gate splits case 1	0.040935	0.275939	0.040935	0.275939	0.275939	0.275939	0.037326	0.005513	0.005513
Gate splits case 2	0.262258	0.0745520	0.02958127	-0.0277864	0.0448917	-0.299859	0.361466	0.370204	0.146059

TABLE SM-1. Parameters of the reduced gates, which were used in the figures.